Journal of Diabetes Science and Technology
Volume 7, Issue 6, November 2013
© Diabetes Technology Society

ORIGINAL ARTICLE

Predicting Glucose Sensor Behavior in Blood Using Transport Modeling: Relative Impacts of Protein Biofouling and Cellular Metabolic Effects

Matthew T. Novak, B.S., Fan Yuan, Ph.D., and William M. Reichert, Ph.D.

Abstract

Background:

Tissue response to indwelling glucose sensors remains a confounding barrier to clinical application. While the effects of fully formed capsular tissue on sensor response have been studied, little has been done to understand how tissue interactions occurring before capsule formation hinder sensor performance. Upon insertion in subcutaneous tissue, the sensor is initially exposed to blood, blood borne constituents, and interstitial fluid. Using human whole blood as a simple *ex vivo* experimental system, the effects of protein accumulation at the sensor surface (biofouling effects) and cellular consumption of glucose in both the biofouling layer and in the bulk (metabolic effects) on sensor response were assessed.

Methods:

Medtronic MiniMed SofSensor glucose sensors were incubated in whole blood, plasma-diluted whole blood, and cell-free platelet-poor plasma (PPP) to analyze the impact of different blood constituents on sensor function. Experimental conditions were then simulated using MATLAB to predict the relative impacts of biofouling and metabolic effects on the observed sensor responses.

Results:

Protein biofouling in PPP in both the experiments and the simulations was found to have no interfering effect upon sensor response. Experimental results obtained with whole and dilute blood showed that the sensor response was markedly affected by blood borne glucose-consuming cells accumulated in the biofouling layer and in the surrounding bulk.

Conclusions:

The physical barrier to glucose transport presented by protein biofouling does not hinder glucose movement to the sensor surface, and the consumption of glucose by inflammatory cells, and not erythrocytes, proximal to the sensor surface has a substantial effect on sensor response and may be the main culprit for anomalous sensor behavior immediately following implantation.

J Diabetes Sci Technol 2013;7(6):1547–1560

Author Affiliation: Department of Biomedical Engineering, Duke University, Durham, North Carolina

Abbreviations: (ANCOVA) analysis of covariance, (PBS) phosphate-buffered saline, (PPP) platelet-poor plasma, (SEM) scanning electron microscope

Keywords: biocompatibility, biomaterials, biosensors, modeling

Corresponding Author: William M. Reichert, Ph.D., Department of Biomedical Engineering, Duke University, 136 Hudson Hall, Box 90281, Durham, NC 27708; email address *reichert@duke.edu*

Introduction

The most prevalent sensor configurations used in glucose monitoring are transcutaneous systems that measure subcutaneous interstitial glucose.[1] In order to bring a mechanistic description to sensor behavior in subcutaneous tissue, we previously presented a computational transport model to elucidate the effects that constituent parts of fully formed capsular tissue have upon a transcutaneous sensor's ability to measure glucose values accurately in real time.[2] However, a more complete understanding of the effects of tissue interactions on sensor function should also include events that occur prior to mature capsule formation. Clinically, this time frame is of particular importance because it coincides with the 3–7 day windows of Food and Drug Administration approval for all commercially available continuous glucose monitoring systems.[3–6]

At insertion, these sensors are rapidly exposed to blood, blood borne constituents, and interstitial fluid from cut vasculature, and the sensor surface becomes fouled with a layer of blood plasma proteins and adhered blood borne cells. Sensor fouling is the first step in the foreign body response, and the following tissue reaction has been posited to decrease glucose concentration near the sensor over time, as well as limit the diffusion of interstitial glucose to the sensor.[7–9] Prichard and coauthors[10] have previously shown that interstitial glucose concentrations decrease around implanted tissue, yet the exact cause of this depletion in early stage tissue reaction is not known.

It has been suggested that protein adsorption and cell adhesion serve as diffusive and consumptive barriers to glucose transport.[11] Klueh and coauthors[11] reported a series of experiments using sensors from both Abbott Diabetes Care and DexCom that examined this interaction by immersing transcutaneous sensors in unheparinized and heparinized whole blood. All of the sensors exhibited a temporal decay in glucose signal, which they attributed to glucose consumption by erythrocytes accumulated at the sensor surface.[11] This group also conducted *in vivo* studies on the role of erythrocyte-embedded clots on sensor function in mice.[12]

Similar to Klueh and coauthors,[11,12] in the current study, the effects of protein biofouling and cellular accumulation on glucose concentration near a sensor were observed experimentally by recording the changes in response of commercially available Medtronic MiniMed SofSensors in heparinized whole blood and various blood constituents. Numerical simulations were then used to further predict mechanistic scenarios that could be used to explain the experimental observations. Our simulations support the conclusion that cellular glucose consumption, not transport resistance due to biofouling, limits glucose concentration near a sensor.

Materials and Methods

Sample Preparation for Whole Blood and Blood Constituent Study

As described in the **Appendix**, blood constituent samples were obtained and prepared through the fractionation of blood via centrifugation using an existing protocol to gather platelet-poor plasma (PPP) for studies.[13,14]

Whole Blood and Platelet-Poor Plasma Studies

All sensors were "precalibrated" as described in the **Appendix**. Once a baseline was obtained, the sensors were transferred from the phosphate-buffered saline (PBS) bath to one of two 10 ml samples of either gently stirred whole blood or PPP at 37 °C. This incubation was carried out until a baseline was formed, which took approximately 10 h. Raw current values were wirelessly transmitted from the sensor to a computer via a proprietary data acquisition program provided by the Medtronic Corporation. During the 10 h incubation, blood and PPP glucose concentrations were measured via test strips to ensure that the sensors were accurately recording trends in each test group. During the 10 h incubation, blood and PPP glucose concentrations were measured periodically via test strips (OneTouch Ultra, Johnson & Johnson, Milpitas, CA) to ensure that the sensors were accurately recording trends in each test group. To examine whether blood and PPP allow sensors to behave in a stepwise, nonreactive fashion like PBS, glucose incursions were made to double the glucose in the system. Sensors were then allowed to gather a baseline over 6 h,

and the process was repeated. Test strip measurements were made at the beginning and the end of each incursion to see if sensor response mimicked a direct blood glucose concentration measurement. After the blood incubation, both sensors were "postcalibrated" in a stirred PBS bath at 37 °C using the same process as the precalibration. This study was repeated three times (n = 3).

Whole and Dilute Blood Study

To examine the effect of cell number and consumption upon sensor readings, sensors were immersed in both whole and dilute blood. After the same PBS calibration step described in Whole Blood and Platelet-Poor Plasma Studies, two sensors were submerged in one of two test solutions. The first solution was heparinized whole blood prepared as described in Sample Preparation for Whole Blood and Blood Constituent Study. The second solution was blood diluted 1:11 in its own PPP, which should not dilute the glucose concentration of the sample while diluting the cell concentration. The sensor treatment protocol followed the same layout as detailed in Whole Blood and Platelet-Poor Plasma Studies. This study was repeated three times (n = 3).

Data Collection, Calibration, and Statistical Analysis

All sensor signals were sorted and plotted using MATLAB (The Mathworks, Natick, MA). Calibration curves were calculated as a linear fit by using the "polyfit" command in MATLAB. Analysis of covariance (ANCOVA) was performed in MATLAB to assess significant differences in the slopes of the linear portions of the sensor signal during incubation in different blood constituents ($p < .05$).

Modeling of Cellular Glucose Consumption

To complement experimental findings, a numerical simulation of the experimental setup was derived and implemented using MATLAB. **Figure 1** presents a schematic representation of the model used in this study, which was modified from the model presented in a previous article by this group.[2] Briefly, transport of glucose through the environment surrounding the sensor was treated as a two-compartment construct. The first compartment, the one closer to the sensor with respect to distance, was the biofouling layer (C_{layer}), a thin layer of proteins and adherent/entrapped cells that forms in within minutes of blood exposure. The second compartment (C_{bulk}) was the bulk blood surrounding the sensor and its biofouling layer. Values for all constants are defined in **Table 1**. Model specifics as well as initial and boundary conditions are described in the **Appendix**.

Table 1.
List of All Baseline Model Parameters

Model parameters	Parameter values		
	Biofouling layer	Bulk blood	Reference
Diffusion coefficient (D) (cm^2/s)	1.87×10^{-6}	3.5×10^{-6}	2
Porosity (ε) (unitless)	0.91	0.55	[a]
Layer thickness (L) (μm)	75	—	2
Michaelis–Menten constant (K_M) (μM)	6.13×10^3	4×10^3	15,16
Maximal rate of cellular glucose uptake (V_{max}) (μmol/cell/s)	$4.88 \times 10^{-11}/1.357 \times 10^{-12}$	1.357×10^{-12}	15,16
Permeability of biofouling layer (P_{layer}) (cm/s)	5×10^{-3}	—	[b]
Conversion constant (λ) (mol/mM/s)	2.574×10^{-14}	—	2
Cell volume (z_{cell}) (liter/cell)	9.5×10^{-13}	—	2
Glucose sensor radius (a) (cm)	0.07	—	2
Sensor surface area (A) (cm^2)	0.0058	—	2

[a] Calculated values with no previous citation.
[b] Model assumptions.

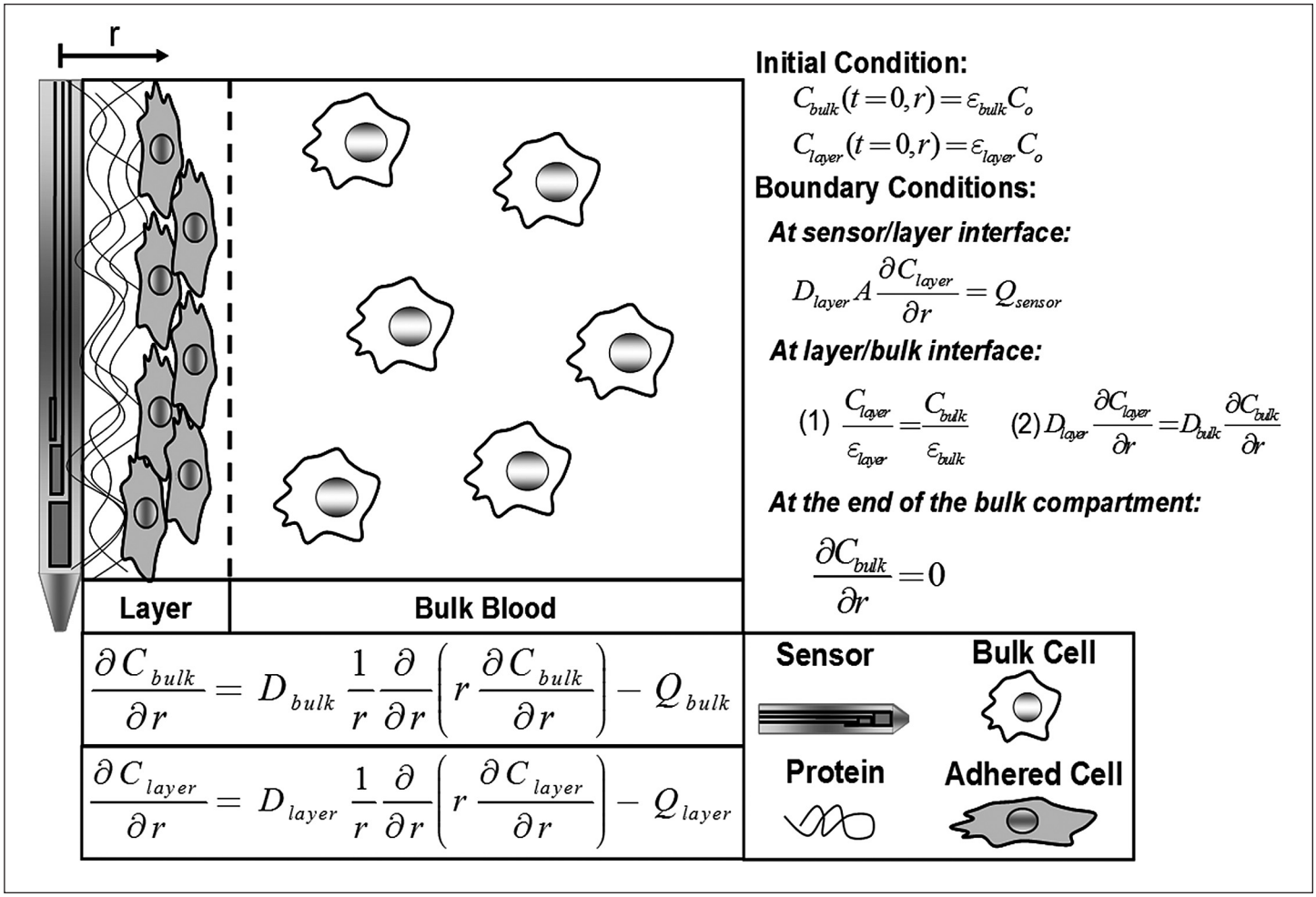

Figure 1. Schematic representation of diffusion through bulk blood and a layer of adsorbed proteins and cells.

Glucose uptake was considered an enzymatically mediated event and was thus modeled using Michaelis–Menten kinetics.[2] These simulations assumed that the glucose-consuming cells in the biofouling layer were, depending on the scenario, either inflammatory cells or erythrocytes, while the cells in the bulk were erythrocytes. Thus the $V_{max,bulk}$ was set to 1.36×10^{-12} μmol/cell/s, the reported value of maximal glucose consumption rate for human erythrocytes, as reported by Yang and coauthors.[15] The baseline $V_{max,layer}$ value used for these calculations was either 4.88×10^{-11} μmol/cell/s as reported by Ahmed and coauthors[16] for glucose uptake by human macrophages during inflammation or the erythrocyte value reported by Yang and coauthors.[15] The V_{max} of the inflammatory cell was chosen to be that of a macrophage, but it is worth noting that other leukocytes such as lymphocytes and neutrophils have similar glucose uptake kinetics.[17,18]

Five computational scenarios (**Table 2**) were examined to compare the effect of glucose consumption by different cell types (inflammatory cell or erythrocyte) within the biofouling layer and the bulk blood. The results of these simulations were then compared directly to two experimentally measured normalized sensor signals in whole blood from **Figure 3** (the maximal decline following addition of the sensor and the minimal decline after a

Table 2.
Outline of Five Different Computational Scenarios for Glucose Transport to an Indwelling Sensor[a]

	Biofouling layer cell type	Bulk blood cell type
Scenario 1	Macrophage	Erythrocyte
Scenario 2	Macrophage	None
Scenario 3	None	Erythrocyte
Scenario 4	Erythrocyte	Erythrocyte
Scenario 5	Erythrocyte	None

[a] To represent these changes in cell type, the Michaelis–Menten kinetic values of V_{max} and K_m were changed accordingly.

glucose addition to show a range of declines) to find which cell type had the dominant effect on decreased sensor signals. To investigate the ability for the proteins within the biofouling layer to act alone as a diffusive barrier for glucose transport to the sensor surface, the simulation was run with both $V_{max,layer}$ and $V_{max,bulk}$ set to zero, creating an *in silico* analog to the PPP s tudies.

Modeling Biofouling Layer Glucose Depletion Zone Formation

To investigate the spatial effect of inflammatory cell aggregation and glucose consumption on sensor readings, glucose concentration profiles were plotted with respect to distance for different values of $V_{max,layer}$. The maximal glucose uptake rate of the cells in the layer ($V_{max,layer}$) was varied among four different values: (1) V_{max} = 0, representative of only an acellular protein biofouling layer; (2) V_{max} for erythrocytes; (3) V_{max} for macrophages; and (4) twice the V_{max} for macrophages. The last case was considered to assess the possible effect of increased cellular accumulation at the sensor interface.

Numerical Methods

Governing partial differential equations in the simulations were discretized into a series of ordinary differential equations using the finite difference method. Differential equations from all earlier studies were solved using the differential equation solver, ode15s, in MATLAB.

Scanning Electron Microscope Imaging of Sensor Surface

The protocol for scanning electron microscope (SEM) was modified from Nurdin and coauthors[19] and is described in the **Appendix**.

Results

Whole Blood, Dilute Blood, and Platelet-Poor Plasma Studies

Figure 2 shows the reproducibility of results from submerging sensors in whole blood. For both trials, signals initially declined upon immersion in whole blood. Moreover, when glucose is added to the system, the signal does not maintain a step increase like in the precalibration immersion in glucose-spiked PBS. Postcalibration steps verified that sensor functionality was maintained throughout the course of the immersion. This anomalous response in whole blood spurred further experiments where sensors were immersed in different blood constituents.

Figure 3 shows mean continuous glucose sensor measurements in whole blood (blue solid trace), PPP (red solid trace), and dilute blood (black solid trace) derived from the same stock of whole blood, as well as discrete glucose concentrations sampled by test strips for each (open circles). After precalibration, one sensor was immersed in PPP and the other was immersed in whole blood. Using ANCOVA, the slope of the initial sensor decline in whole blood was found to be statistically significantly different from the initial decline in the PPP case. Doubling the whole blood glucose at 16 and 24 h caused jumps in sensor signal followed again by signal decays that were also statistically significant from their complementary PPP traces. Even though the magnitude of the corresponding test strip glucose concentrations was always lower, it is important to note that the slopes of the signal declines were found to be not statistically significant from the corresponding test strip measurements.

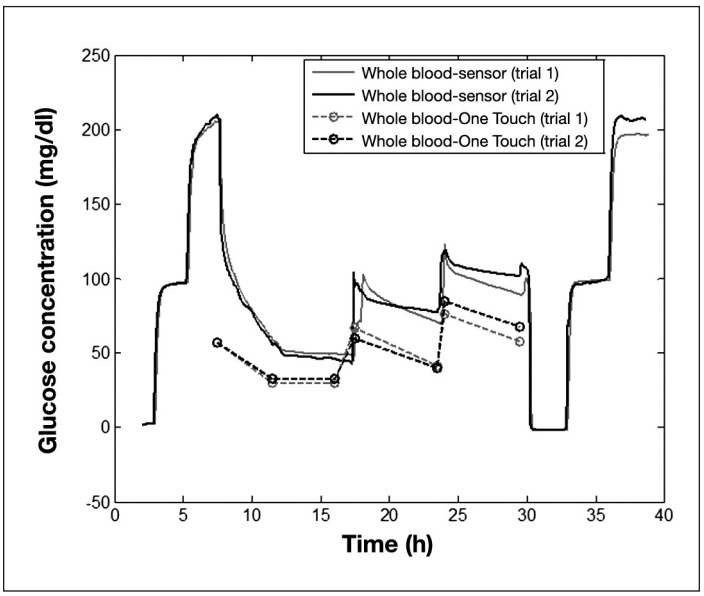

Figure 2. Incubation of Medtronic MiniMed sensors in whole blood.

The PPP-immersed sensor behaved essentially as if it was immersed in PBS. This finding suggests that no glucose was being removed from the system in PPP and that adsorption of plasma proteins to the sensor surface during whole blood immersion was not contributing to the decreased sensor response in whole blood. Because the only difference between PPP and whole blood is the population of cells, the observed declines in whole blood sensor signal relative to PPP would be the result of cells within the system consuming glucose.

The sensor in PPP-diluted blood exhibited an intermediate sensor response when compared with the whole blood case. Similar to the sensor in whole blood, the sensor in PPP-diluted whole blood exhibited signal declines upon immersion and following glucose bolus additions, albeit with slopes significantly less than whole blood for all three cases of decline ($p < .05$). These results indicate that the cells in PPP-diluted blood were also consuming glucose but to a lesser extent than in whole blood, presumably due to the effects of dilution, further demonstrating the effects of cellular consumption on sensor signal. These findings were also corroborated by test strip measurements at discrete time points.

Numerical Modeling

The dashed lines in **Figure 4** display the maximal and minimal fractional experimental signal declines as derived from the data in **Figure 3**, where the sharper decline occurred following the initial sensor immersion and the shallower decline occurred following an addition of glucose. The shaded grey space between them is meant to represent the range of sensor declines observed when immersed in whole blood. The solid lines in **Figure 4** are simulated fractional declines in sensor signal with respect to time for cases of five distinct scenarios of cellular presence around the sensor (**Table 2**).

The erythrocyte-only simulations—be they in the bulk (red), in the layer (cyan), or both (black)—all underestimate the initial ~60% sensor decline following the sensor immersion in whole blood and the ~40% experimental decline post-glucose addition. However, when the simulations include just adherent leukocytes, the simulations lie within the range of experimental sensor declines in whole blood. The simulation with adherent macrophages and bulk erythrocytes overestimates both experimental declines. These data suggest that adherent leukocytes are more likely the primary mitigators of the initial sensor decline and not adherent erythrocytes as suggested by Klueh and coauthors.[11,12]

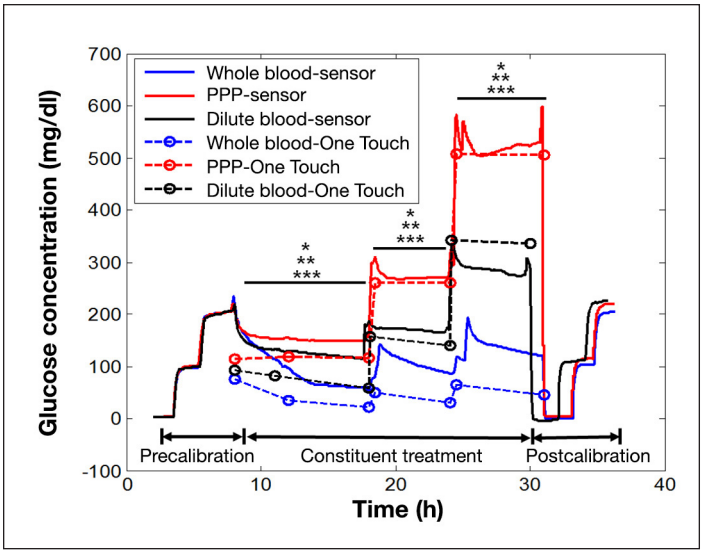

Figure 3. Comparison of mean glucose sensor readings in PPP (red), whole blood (blue), and dilute blood (black) as a function of time ($n = 3$). Sensor readings are corroborated by OneTouch readings for each (circles in dashed line). *Statistically significant differences in slopes of sensor signals between whole blood and PPP incubations ($p < .05$). **Statistically significant differences in slopes of sensor signals between dilute blood and PPP incubations ($p < .05$). ***Statistically significant differences in slopes of sensor signals between dilute blood and whole blood incubations ($p < .05$).

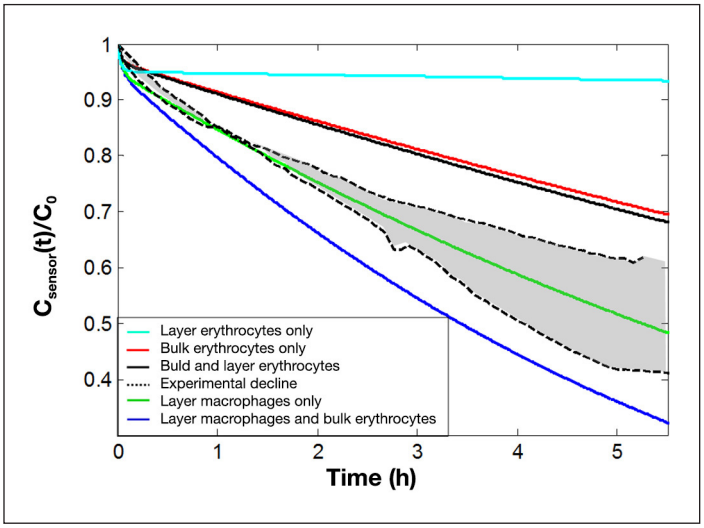

Figure 4. Simulated sensor reading as a function of time. The ordinate is represented as the fraction of initial glucose in the system and the abscissa is time in hours. The simulation compares five different scenarios against the range of maximal and minimal experimental sensor declines in whole blood from **Figure 3** (shaded grey area bounded by dotted lines) to determine which group of cells contributes most to glucose depletion in each case. Scenario 1 (blue line) is represented by the presence of macrophages in the layer and erythrocytes in the bulk. Scenario 2 (green line) is represented by the presence of only macrophages in the layer and no cells in the bulk. Scenario 3 (red line) is represented by the presence of only erythrocytes in the bulk with no macrophages in the layer. Scenario 4 (black line) is represented by the presence of only erythrocytes in both the bulk and the layer. Scenario 5 (cyan line) is represented by the presence of only erythrocytes in the layer and no cells in the bulk.

The trends in **Figure 4** suggest that the cell-embedded biofouling layer may result in the formation of a glucose depletion zone adjacent to the sensor surface. **Figure 5** contains a family of normalized glucose concentration profiles as a function of distance extending from the sensor surface through a representative 75 μm thick biofouling layer. When erythrocytes exist as the only cell type within the biofouling layer (black dot), the radial decrease in glucose concentration relative to the initial concentration is imperceptible, with a decrease of 9×10^{-5}%. This finding is nearly identical to the case where $V_{max,layer} = 0$ (red squares), representing an acellular protein biofouling layer. However, when macrophages are the only cell type within the biofouling layer and $V_{max,layer} = V_{max}$ for macrophages (blue dot), glucose concentrations do decrease toward the sensor surface, with concentrations dropping by 4% over the length scale. Moreover, a doubling of the macrophage V_{max} within the layer (blue circle), which is meant to represent the increased presence of inflammatory cells at the site of implantation, increased the magnitude of depletion by causing concentrations to drop by 8% over the length scale.

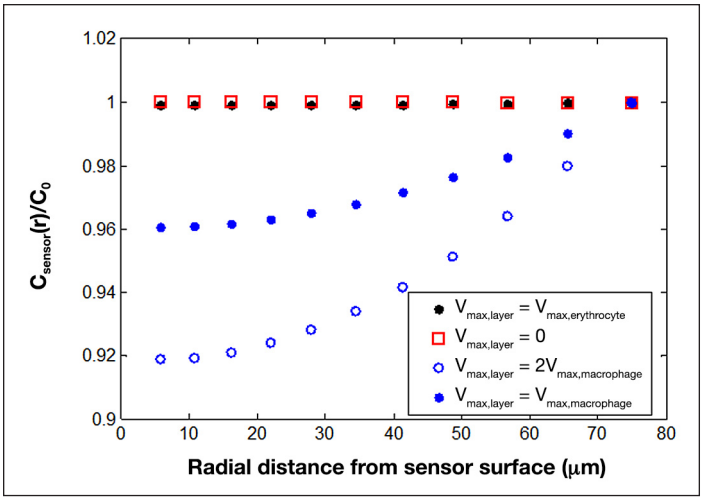

Figure 5. Simulated effects of adherent cell aggregation and glucose consumption on glucose concentration at the sensor surface as a function of distance. Increases in cell presence were modeled as an increase in $V_{max,layer}$ within the layer. When macrophages are the sole cell type in the adherent layer (blue filled circle), there is a depletion of glucose with respect to distance. This depletion increases as the number of macrophages increases, which is denoted by an increase in $V_{max,layer}$ (blue open circle). When the adherent layer is populated by only erythrocytes (black filled circle), there is close to no radial depletion. This is similar to the acellular case where $V_{max,layer} = 0$ (red open square), indicating only a biofouling layer. Data are presented as fractional signal decline.

Figure 6 displays a simulated fractional decline in sensor signal caused by the presence of an acellular protein adsorption layer with respect to time set against experimental sensor data from **Figure 3** (black dashed line). Assuming a representative fibrin mat porosity of 0.91, the decrease in glucose concentration with respect to time across the protein film was negligible. Dramatically decreasing the porosity to a much lower value of 0.1 had more pronounced, but still small, temporal effect on glucose transport to the sensor (>90% of the original value). Taken together, these results show that the protein film itself does not restrict the transport of glucose to the sensor surface.

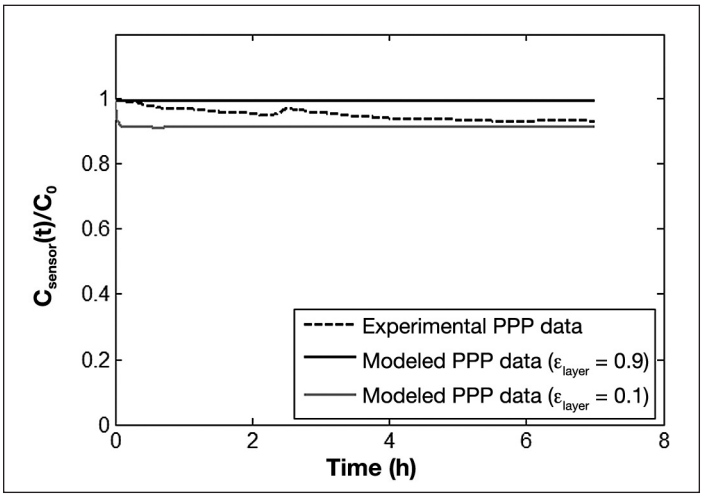

Figure 6. Simulated effects of the acellular biofouling layer as a diffusive barrier with respect to time. Data are presented as a fractional signal decline.

Discussion

The current study employed well-stirred whole blood as a simple *ex vivo* living system to approximate the environment in the first few hours of sensor implantation when bleeding, hemostasis, and the adhesion of blood borne cells are dominant events around the sensor surface. The use of whole blood and PPP allowed for the separation of transport effects from metabolic effects arising from the accumulation of blood plasma proteins and blood borne cells at the sensor surface.

Trends in sensor values were compared across sensors by converting all sensor readouts from current to concentration. Postcalibration of sensors removed from whole blood or PPP as well as periodic glucose sampling taken with glucose test strips ensured that changes in sensor readings were an accurate reporting of glucose concentration in the surrounding milieu.

Figure 3 compares glucose readings for sensors immersed in whole blood, PPP, and diluted whole blood. With each addition of glucose into PPP, both the sensor and test strip readings registered steady step increases in glucose concentration. The results from the PPP incubation study were corroborated by a numerical simulation showing that the biofouling layer had little effect in limiting glucose transport to the sensor with respect to time (**Figure 6**). This behavior in PPP was akin to measurements in buffered glucose solution, suggesting that the fouling of sensors by blood plasma proteins like those seen in the SEM image of **Figure 7D** was having no effect on the decrease in sensor signal.

In contrast, the sensor and test strip readings in whole blood registered sharp increases followed by declines following initial immersion and additions of glucose. Sensors in diluted whole blood exhibited a combination of step increases and signal declines intermediate between that observed for PPP and whole blood. Clearly, exposure to blood caused a decrease in blood glucose concentration that did not result from the accumulation of blood plasma proteins at the sensor surface or from a failure of the sensor to accurately read glucose; rather, these declines arose from a combination of sensor equilibration and cellular glucose consumption. As sensor output could be modulated by the concentration of cells within the blood, the role of cellular presence on sensor signal is apparent.

The ratio for erythrocytes to leukocytes in whole blood is roughly 1000:1, and as such, the SEM images of the biofouled sensor surface (**Figure 7**) showed many more erythrocytes than leukocytes, but clearly not three orders of magnitude more.[20] In spite of their larger number, erythrocytes do not exhibit substantial metabolic requirements on a per-cell

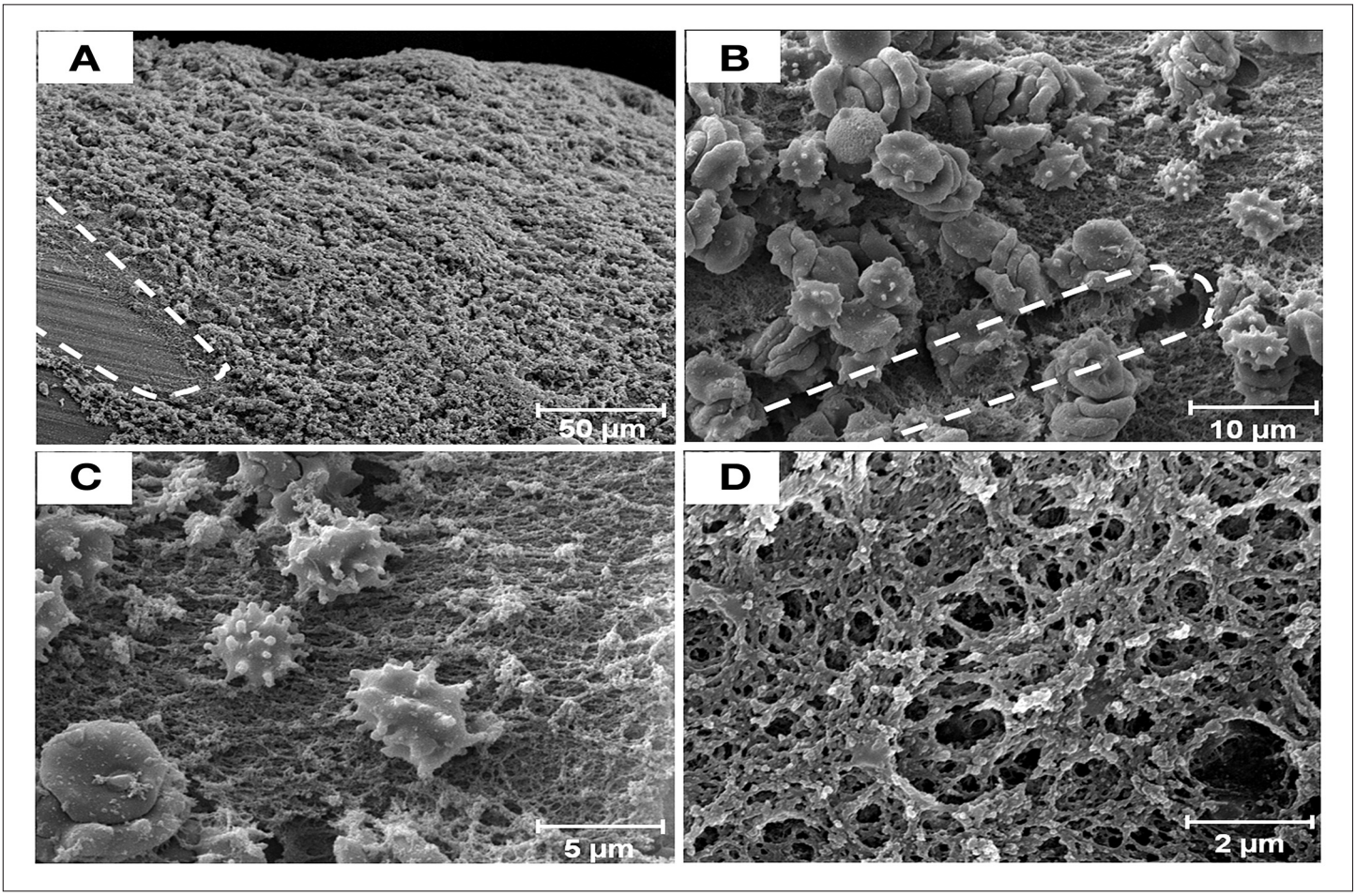

Figure 7. (A,B) The SEM images of a blood clot on a sensor surface (1000x, 5000x). **(C)** The SEM images of leukocyte adhesion on the sensor surface (10000x). **(D)** The SEM image of protein adsorption layer on the sensor surface (20000x). (A) The difference between regions covered in protein and cells and the bare sensor surface (outlined by dashed line). Note the infiltration of the active sensing region by cells and proteins in **B** (sensing region outlined by a dashed line).

basis, as their net efflux of glucose is roughly that of the net influx.[20–23] In contrast, activated immune cells have significant glucose demands.[24,25] Therefore, it is reasonable to infer that accumulation of the more metabolically active leukocytes could more significantly affect the glucose concentration measured by the sensor. As **Figure 4** demonstrates, the simulation that comprises adherent macrophages in the biofouling layer lies within the range of experimentally observed sensor declines. This suggests that inflammatory cells like macrophages, although fewer in number than erythrocytes, are the main determinant for a decrease in sensor signal with respect to time. It should be noted, however, that bulk erythrocytes, due to their sheer number in blood, still consume a significant amount of glucose. However, the computational scenarios where only erythrocytes were present all underestimated the experimental sensor declines in whole blood.

Figure 5 further extends this conclusion by simulating the ability of erythrocytes and macrophages to induce a "glucose depletion zone" within the vicinity of the sensor surface. When erythrocytes exist as the only cell type within the biofouling layer, the radial glucose concentration does not appreciably decrease, making it indistinguishable from the acellular case. Through this comparison, it is evident that erythrocytes do not create a glucose depletion zone. However, when macrophages are considered the only cell type in the layer, depletion occurs with the magnitude of depletion increasing with increasing cellular presence. While the macrophage-mediated cases produce seemingly modest depletions, it should be noted that the time at which these radial concentrations were taken is merely hours after immersion of the sensor in whole blood. In an *in vivo* setting, this depletion, in turn, will inhibit the sensor from being able to accurately measure a patient's interstitial glucose.

Simulations were run to assess if the cellular component of the biofouling layer may have imposed some resistance to glucose transport. This increase in resistance due purely to the steric effects of cell presence was addressed in **Figure 6**, where the porosity is decreased from 0.9 to 0.1. Even in this case, a steady state value of greater than 90% of the original glucose concentration was maintained throughout the length of the simulation. Such a finding suggests that while the presence of cells can confer transport resistance, the effects of this resistance are small compared with the consumptive effects seen in **Figures 4** and **5**.

Given the long-standing uncertainty of how the *in vivo* environment affects glucose sensor function, the current study provides a clearer picture of how protein and cell accumulation at the sensor surface affects sensor performance in a living milieu. The whole blood, dilute blood, and PPP studies in concert with the numerical findings suggest that while the sensors accurately measure the glucose that is able to freely diffuse to them, glucose consumption by inflammatory cells accumulated at the sensor surface consume the analyte before it can reach the sensor, thereby limiting sensing capability.

Finally, this study does come with two caveats. First, it only considers the resistance to glucose transport as a mitigating factor in anomalous sensor response. However, glucose oxidase can only produce hydrogen peroxide when in the presence of oxygen. The concentration of unbound oxygen in tissue is much lower than that of glucose, meaning that oxygen could be the rate limiting input to sensor function.[26,27] Furthermore, tissue wounded from implantation has been shown to have decreased oxygen tension relative to untreated tissue.[28] Much like with glucose, inflammatory cells have elevated capacity for oxygen consumption to facilitate antimicrobial defense mechanisms like respiratory burst.[29] While the goal of this study is to focus upon factors that would limit only glucose transport, future studies should investigate the role of limited oxygen supply in decreased sensor function. Second, the sensors used in this study are specifically intended for insertion into subcutaneous tissue for continuous monitoring of interstitial glucose and were not designed for sensing glucose in bulk blood. That said, these sensors accurately tracked accessible glucose in well-stirred whole blood and performed robustly throughout the study.

Conclusions

Whole blood, diluted whole blood, and PPP experiments indicated that decreases in sensor signal were attributable to the presence of glucose-consuming inflammatory cells proximal to the sensor surface. Moreover, the biofouling layer of adsorbed proteins on the sensor surface was shown to have no contribution to sensor signal declines.

Computer simulations supported the experimental findings by demonstrating the effect that an aggregation of adhered cells has on creating a "glucose depletion zone" of glucose proximal to the sensor surface. The results of this body of work demonstrate that instead of sensors failing, as is often reported in the literature, implant-associated changes in the local environment are creating a scenario that inhibits otherwise functioning sensors from accurately sampling ambient interstitial glucose concentrations.

Funding:

This work was supported by a National Institutes of Health (NIH) Biotechnology Predoctoral Fellowship to Matthew T. Novak (GM T328555) and by an NIH grant (DK 54932) to William M. Reichert.

Acknowledgments:

We gratefully acknowledge Rajiv Shah and Larry Wang of Medtronic MiniMed of Northridge, CA, for the generous donation of sensors used in this study and for many fruitful discussions. We are also thankful for the advice and counsel of Uli Kleuh of the University of Connecticut, and Duke colleagues Michael Nichols, Charles S. Wallace, and Robert Kirkton.

References:

1. Koschinsky T, Heinemann L. Sensors for glucose monitoring: technical and clinical aspects. Diabetes Metab Res Rev. 2001;17(2):113–23.
2. Novak MT, Yuan F, Reichert WM. Modeling the relative impact of capsular tissue effects on implanted glucose sensor time lag and signal attenuation. Anal Bioanal Chem. 2010;398(4):1695–705.
3. Ginsberg BH. The FDA Panel advises approval of the first continuous glucose sensor. Diabetes Technol Ther. 1999;1(2):203–4.
4. Mastrototaro JJ. The MiniMed continuous glucose monitoring system. Diabetes Technol Ther. 2000;2 Suppl 1:S13–8.
5. Garg SK. The future of continuous glucose monitoring. Diabetes Technol Ther. 2009;11 Suppl 1:S1–3.
6. Skyler JS. Continuous glucose monitoring: an overview of its development. Diabetes Technol Ther. 2009;11 Suppl 1:S5–10.
7. Sharkawy AA, Klitzman B, Truskey GA, Reichert WM. Engineering the tissue which encapsulates subcutaneous implants. II. Plasma-tissue exchange properties. J Biomed Mater Res. 1998;40(4):586–97.
8. Wisniewski N, Klitzman B, Miller B, Reichert WM. Decreased analyte transport through implanted membranes: differentiation of biofouling from tissue effects. J Biomed Mater Res. 2001;57(4):513–21.
9. Sharkawy AA, Klitzman B, Truskey GA, Reichert WM. Engineering the tissue which encapsulates subcutaneous implants. I. Diffusion properties. J Biomed Mater Res. 1997;37(3):401–12.
10. Prichard HL, Schroeder T, Reichert WM, Klitzman B. Bioluminescence imaging of glucose in tissue surrounding polyurethane and glucose sensor implants. J Diabetes Sci Technol. 2010;4(5):1055–62.
11. Klueh U, Liu Z, Ouyang T, Cho B, Feldman B, Henning TP, Kreutzer D. Blood-induced interference of glucose sensor function *in vitro*: implications for *in vivo* sensor function. J Diabetes Sci Technol. 2007;1(6):842–9.
12. Klueh U, Liu Z, Feldman B, Henning TP, Cho B, Ouyang T, Kreutzer D. Metabolic biofouling of glucose sensors *in vivo*: role of tissue microhemorrhages. J Diabetes Sci Technol. 2011;5(3):583–95.
13. Hirsh J, Anand SS, Halperin JL, Fuster V; American Heart Association. Guide to anticoagulant therapy: heparin : a statement for healthcare professionals from the American Heart Association. Circulation. 2001;103(24):2994–3018.
14. Weibrich G, Kleis WK, Hafner G, Hitzler WE, Wagner W. Comparison of platelet, leukocyte, and growth factor levels in point-of-care platelet-enriched plasma, prepared using a modified Curasan kit, with preparations received from a local blood bank. Clin Oral Implants Res. 2003;14(3):357–62.
15. Yang H, Wang D, Engelstad K, Bagay L, Wei Y, Rotstein M, Aggarwal V, Levy B, Ma L, Chung WK, De Vivo DC. Glut1 deficiency syndrome and erythrocyte glucose uptake assay. Ann Neurol. 2011;70(6):996–1005.
16. Ahmed N, Kansara M, Berridge MV. Acute regulation of glucose transport in a monocyte-macrophage cell line: Glut-3 affinity for glucose is enhanced during the respiratory burst. Biochem J. 1997;327 (Pt 2):369–75.
17. Nefesh I, Bauskin AR, Alkalay I, Golembo M, Ben-Neriah Y. IL-3 facilitates lymphocyte hexose transport by enhancing the intrinsic activity of the transport system. Int Immunol. 1991;3(8):827–31.
18. Tan AS, Ahmed N, Berridge MV. Acute regulation of glucose transport after activation of human peripheral blood neutrophils by phorbol myristate acetate, fMLP, and granulocyte-macrophage colony-stimulating factor. Blood. 1998;91(2):649–55.
19. Nurdin N, François P, Mugnier Y, Krumeich J, Moret M, Aronsson BO, Descouts P. Haemocompatibility evaluation of DLC- and SiC-coated surfaces. Eur Cell Mater. 2003;5:17–28.
20. Turgeon ML. Clinical hematology: theory and procedures. 4th ed. Philadelphia: Lippincott Williams and Wilkins; 2005.

21. Carruthers A, Melchior DL. Transport of alpha- and beta-D-glucose by the intact human red cell. Biochemistry. 1985;24(15):4244–50.

22. Carruthers A. Facilitated diffusion of glucose. Physiol Rev. 1990;70(4):1135–76.

23. Cloherty EK, Levine KB, Carruthers A. The red blood cell glucose transporter presents multiple, nucleotide-sensitive sugar exit sites. Biochemistry. 2001;40(51):15549–61.

24. Rist RJ, Jones GE, Naftalin RJ. Effects of macrophage colony-stimulating factor and phorbol myristate acetate on 2-D-deoxyglucose transport and superoxide production in rat peritoneal macrophages. Biochem J. 1991;278 (Pt 1):119–28.

25. Kiyotaki C, Peisach J, Bloom BR. Oxygen metabolism in cloned macrophage cell lines: glucose dependence of superoxide production, metabolic and spectral analysis. J Immunol. 1984;132(2):857–66.

26. Leypoldt JK, Gough DA. Model of a two-substrate enzyme electrode for glucose. Anal Chem. 1984;56(14):2896–904.

27. Gough DA, Lucisano JY, Tse PH. Two-dimensional enzyme electrode sensor for glucose. Anal Chem. 1985;57(12):2351–7.

28. Gough DA, Kumosa LS, Routh TL, Lin JT, Lucisano JY. Function of an Implanted Tissue Glucose Sensor for More than 1 Year in Animals. Sci Transl Med. 2010;2(42):42ra53.

29. Babior BM. Oxygen-dependent microbial killing by phagocytes (first of two parts). N Engl J Med. 1978;298(12):659–68.

Appendix

Blood Sample Preparation

In accordance with institutional review board protocol 2257-08-1R17ER, samples of human blood from healthy volunteers were collected in 10 ml vacutainers containing ethylenediaminetetraacetic acid to prevent immediate coagulation. Upon collection, samples were immediately used for studies, as platelet counts have been shown to decrease by over 50% after 72 h *ex vivo*.[A1] Extra measure was taken to further ensure that no coagulation takes place by adding a heparin sulfate stock solution at 100 U/ml in phosphate-buffered saline (PBS; -/-) to the blood to achieve a final heparin concentration of 5 U/ml. This final concentration is higher than the recommended dosage for treatment of 0.4 U/ml to ensure a well-stirred solution for the subsequent long-term studies.[A2]

Blood constituent samples were prepared through the fractionation of blood via centrifugation using an existing protocol from Weibrich and coauthors[A3] to gather platelet-rich plasma and PPP for studies. Platelet-rich plasma is the volume of blood that is absent erythrocytes and leukocytes but contains platelets, small molecules, and plasma proteins. Platelet-poor plasma, however, contains only small molecules and plasma proteins. Platelet-rich plasma was obtained from centrifuging whole blood for 10 min at 1500 rpm and then removing the hematocrit. Platelet-poor plasma was obtained from centrifuging PRP for 15 min at 3600 rpm to remove the platelets. By having different constituents of blood, the contributions of both the plasma and whole blood to sensor function could be delineated.

Plasma-diluted blood was prepared as a 1:11 dilution of whole blood in its own plasma. This produced a cell concentration of 5×10^5 cells/ml, which is a common value for white blood cell concentrations in whole blood.[A4] Platelet-poor plasma was chosen for the blood diluent, as it should not dilute the glucose concentration of the sample while diluting the cell concentration.

Sensor Calibration

Two Medtronic SofSensors were first immersed in a stirred PBS bath at 37 °C initially at 0 mg/dl glucose. To calibrate each sensor, glucose was added to increase the concentration to 100 mg/dl, and a baseline current was allowed to form. This step was then repeated for 200 mg/dl of glucose. From these three data points (0, 100, and 200 mg/dl glucose), a linear calibration curve relating glucose concentration to sensor output current could be made. Besides allowing for concentration readings, this calibration step served as a check that the sensors were properly working, as the sensors were reported by the manufacturer to have a linear response to glucose incursions for a range of 0–400 mg/dl glucose.

Numerical Modeling: Governing Equations

The governing equation describing glucose concentration in the cellular region of the biofouling layer (C_{layer}) is a nonlinear, unidimensional diffusion-reaction equation in cylindrical coordinates through a porous medium. It has a diffusion term and a sink term to describe uptake by adherent cells:

$$\frac{\partial C_{layer}(r,t)}{\partial t} = \frac{D_{layer}}{r}\frac{\partial}{\partial r}\left(r\frac{\partial C_{layer}(r,t)}{\partial r}\right) - Q_{layer}(r,t). \quad (1)$$

Q_{layer} is defined as the rate of glucose uptake by cells in the layer and is modeled by Michaelis–Menten kinetics, where $V_{max,layer}$ is the maximum rate of consumption (nanomoles per cell per second), $K_{M,layer}$ is the Michaelis–Menten constant (nanomoles per liter), ε_{layer} is the porosity of the biofouling layer (unitless), and z_{cell} is the volume of a cell within the layer (liters per cell) [**Equation (2)**]. In this model, the fibrin network and cells were assumed to be well mixed within the biofouling layer. Therefore, they were not considered separately.

$$Q_{layer}(r,t) = \frac{V_{max,layer}C_{layer}(r,t)}{K_{M,layer}\varepsilon_{layer}}\left(\frac{1-\varepsilon_{layer}}{z_{cell}}\right) \quad (2)$$

The governing equation for glucose concentration in the bulk blood (C_{bulk}) is a nonlinear, unidimensional diffusion-reaction equation in cylindrical coordinates through a porous medium:

$$\frac{\partial C_{bulk}(r,t)}{\partial t} = \frac{D_{bulk}}{r}\frac{\partial}{\partial r}\left(r\frac{\partial C_{bulk}(r,t)}{\partial r}\right) - Q_{bulk}(r,t). \quad (3)$$

Q_{bulk} represents the consumption rate of glucose by native red blood cells in the bulk space and is modeled with Michaelis–Menten kinetics as well, where $V_{max,bulk}$ is the maximum rate of glucose consumption (nanomoles per cell per second), $K_{M,bulk}$ is the Michaelis–Menten constant (nanomoles per liter), ε_{bulk} is the porosity of the blood (unitless), and z_{cell} is the volume of a red blood cell [liters per cell; **Eq. (4)**]. This term represents a glucose sink, as uptake of the analyte by cells removes it from the system.

$$Q_{bulk}(r,t) = \frac{V_{max,bulk}C_{bulk}(r,t)}{K_{M,bulk}\varepsilon_{bulk}}\left(\frac{1-\varepsilon_{bulk}}{z_{cell}}\right) \quad (4)$$

The porosity of the acellular biofouling layer (ε_{layer}) was calculated using the specific hydraulic permeability (k) of a fibrin network, which has been reported by Carr and coauthors[A5] to be within the range of 2 to 7 × 10^{-10} cm^2. For a network of randomly oriented fibers, the specific hydraulic permeability is calculated with **Equations (5)** and **(6)**, where ε is ε_{layer} for the simplification of the equation description.[A6]

$$k = \frac{r_f^2\varepsilon^3}{4G(\varepsilon)(1-\varepsilon)^2} \quad (5)$$

$$G(\varepsilon) = \frac{2\varepsilon^3}{3(1-\varepsilon)}\left\{\frac{1}{-2ln(1-\varepsilon) - 3 + 4(1-\varepsilon) - (1-\varepsilon)^2} + \frac{2}{-ln(1-\varepsilon) - \frac{[1-(1-\varepsilon)^2]}{[1+(1-\varepsilon)^2]}}\right\}. \quad (6)$$

As the radius of a fibrin strand (r_f) is known to be 150 nm, ε_{layer} can be found for the range of reported k.[A7] For the model, ε_{layer} was chosen to be 0.91, as it represented a midpoint of the calculated porosity values. The porosity of the bulk space, ε_{bulk}, was set to be 0.55, one minus the volume fraction occupied by the hematocrit (45% of the volume of blood).

Numerical Modeling: Initial and Boundary Conditions

For the initial condition, it was assumed that the diffusion time in the biofouling layer was much shorter than the time scale of simulation. Therefore, the initial condition for the system was a uniform glucose concentration (C_O) multiplied by the porosities of each compartment when the sensor is inserted into the blood at t = 0 s, a plausible assumption, as there was no other intrinsic source of glucose once a sample of blood is taken for an experiment. The boundary condition at the sensor/layer interface was that the flux of glucose diffusion in the biofouling layer times the surface area (A) was equal to the rate of glucose uptake by the sensor, Q_{sensor}. At the interface of the biofouling layer and bulk regions, it was assumed that there was no consumption or accumulation of glucose, so the concentrations normalized by the porosities and fluxes were continuous across the interface. No flux boundary conditions were assigned to the outer boundary condition at the end of the bulk compartment, because glucose could not move into or out of the boundary at the edge of the beaker, creating an insulating boundary and making the flux at the outer boundary equal to zero.

Scanning Electron Microscope Imaging

Clean Medtronic MiniMed SofSensors were incubated in freshly collected whole blood and PPP treated in the manner described in Sample Preparation for Whole Blood and Blood Constituent Study for 24 h at 37 °C. After the end of the incubation period, the sensor tips were fixed in 1.5% glutaraldehyde in PBS for 4 h at room temperature. The samples were subjected to a series of dehydration steps in solutions of ethanol of increasing concentration before treatment with tetramethylsilane. The treated sensor underwent gold sputter coating to a thickness of 7 μm before being imaged on a scanning electron microscope (FEI XL30 SEM-FEG).

References:

A1. Hartley PS, Savill J, Brown SB. The death of human platelets during incubation in citrated plasma involves shedding of CD42b and aggregation of dead platelets. Thromb Haemost. 2006;95(1):100–6.

A2. Hirsh J, Anand SS, Halperin JL, Fuster V; American Heart Association. Guide to anticoagulant therapy: heparin : a statement for healthcare professionals from the American Heart Association. Circulation. 2001;103(24):2994–3018.

A3. Weibrich G, Kleis WK, Hafner G, Hitzler WE, Wagner W. Comparison of platelet, leukocyte, and growth factor levels in point-of-care platelet-enriched plasma, prepared using a modified Curasan kit, with preparations received from a local blood bank. Clin Oral Implants Res. 2003;14(3):357–62.

A4. Turgeon ML. Clinical hematology: theory and procedures. 4th ed. Philadelphia: Lippincott Williams and Wilkins; 2005.

A5. Carr ME Jr, Shen LL, Hermans J. Mass-length ratio of fibrin fibers from gel permeation and light scattering. Biopolymers. 1977;16(1):1–15.

A6. Truskey GA, Yuan F, Katz DF. Transport phenomena in biological systems. 1st ed. Upper Saddle River: Pearson Prentice Hall; 2004.

A7. Collet JP, Shuman H, Ledger RE, Lee S, Weisel JW. The elasticity of an individual fibrin fiber in a clot. Proc Natl Acad Sci U S A. 2005;102(26):9133–7.